

Phase field study of precipitate growth: Effect of misfit strain and interface curvature

R. Mukherjee, T. A. Abinandanan^{*}, M. P. Gururajan

*Department of Materials Engineering, Indian Institute of Science, Bangalore,
India*

Abstract

We have studied diffusion controlled growth of an isolated, misfitting precipitate in a supersaturated matrix using a phase field model. Treating our simulations as computer experiments, we have critically compared our simulation results with those from Zener-Frank and Laraia-Johnson theories for the growth of non-misfitting and misfitting precipitates, respectively. The agreement between simulations and the ZF theory is very good for 1D systems. In 2D systems with interfacial curvature, we still get good agreement between simulations and both ZF and LJ theories, but only for large supersaturations. At small supersaturations, the growth coefficient from our simulations does not converge towards that from theory, but a large gap does remain when the simulations end due to overlap of diffusion fields. An interesting finding from the simulations is the less complete realization of the Gibbs-Thomson effect during growth, particularly in more supersaturated alloys. Thus, even at the same precipitate size, the curvature effects are less severe in more supersaturated alloys.

Key words: phase field models, Microstructure, Phase Transformations, precipitation

PACS: 61.72.-y, 46.25.-y, 81.30.Mh

1 Introduction

In their classic study of diffusional growth of an isolated precipitate into a supersaturated matrix, Zener [1] and Frank [2] established the parabolic growth law: the square of the precipitate size (radius) increases linearly with time. They used what is now referred to as a 'sharp interface' model. Fig. 1 shows a schematic of a composition profile in the precipitate p and matrix m phases during growth. Local equilibrium at the (sharp) interface yields the matrix interfacial composition, c_I^m , which is used as a boundary condition for solving the diffusion equation; the far-field composition, c_∞ is the other boundary condition. Neglecting interface curvature (capillarity) effects, c_I^m is the same as c_e^m , the equilibrium matrix composition obtained from the phase diagram, and the precipitate grows under a supersaturation of $(c_\infty - c_e^m)$.

The Zener-Frank (ZF) theory was extended by Laraia and Johnson (LJ) to diffusional growth of elastically misfitting precipitates; the work of LJ built on the work of Eshelby [3], Larche and Cahn [4–7], Johnson and Alexander [8] and Leo and Sekerka [9]. The main result of the LJ study is that the parabolic growth law continues to be valid for precipitates with misfit, but the growth coefficient depends on (a) misfit, (b) elastic moduli of the two phases and (c) interfacial stress and (d) compositional stress.

In the sharp interface model used by LJ, the effect of dilatational misfit (without capillary effects) is to raise the matrix interfacial composition from c_e^m to c_E^m , and therefore, to decrease the supersaturation (by a constant factor) to $c_\infty - c_E^m$. Thus, the LJ theory predicts that the growth coefficient α in misfit-

* Corresponding author

Email address: abinandanan@gmail.com (M. P. Gururajan).

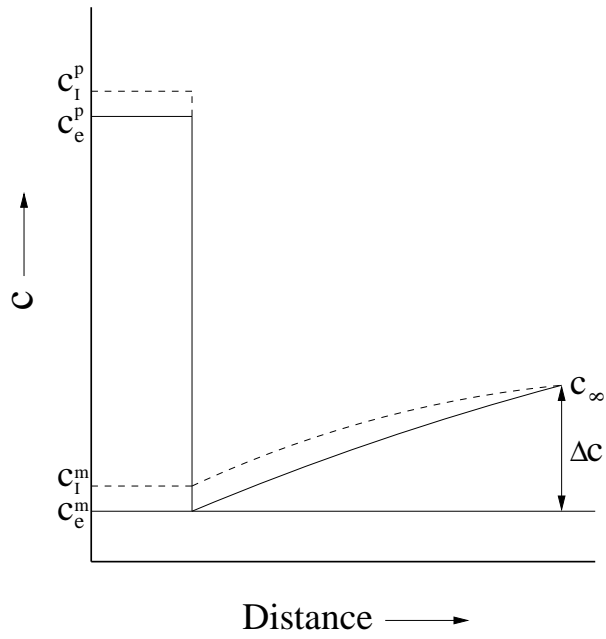
ting systems is the same as that in non-misfitting systems with $(c_\infty - c_E^m)$ as the supersaturation. This conclusion is valid for systems in which diffusivity is independent of the state of stress; our study is restricted to these systems (as already mentioned, LJ have studied other stress-induced effects).

Direct experimental verification of the LJ results is extremely difficult, not only due to the ‘isolated particle’ assumption, but also due to lack of reliable data on stress effects on diffusion. Moreover, the assumption of isotropic interfacial energy may also be difficult to realize experimentally in crystalline alloys. Thus, simulations can act as ‘computer experiments’ for validating the LJ results, since their parameters can be so tuned to make the computational model resemble that used in the LJ theory as closely as possible. Thus, the first goal of our study is a critical comparison of the sharp interface results of LJ with those from our simulations based on a (diffuse interface) phase field model.

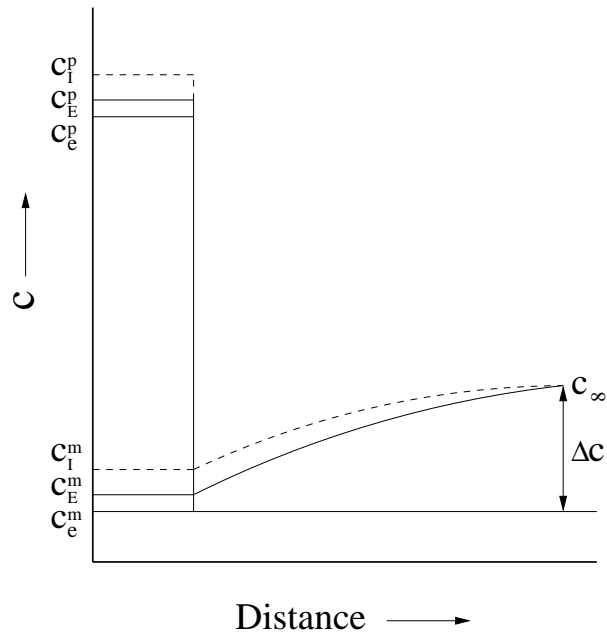
In ZF and LJ theories, which neglect interface curvature effect, the diffusion fields at different times are self-similar. This self-similarity is broken when capillarity effect is included, since c_I^m (in Fig. 1a and b) is size dependent. Capillarity, then, not only decreases the growth rate α , but also renders it size-dependent. The second goal of this study is to evaluate the extent of this reduction in α with a view to identifying the supersaturation and precipitate size regimes in which it is likely important.

Our results also allow us to address two other issues:

(a) Our simulation results on systems with low supersaturation can be used to verify the predictions of Johnson and Alexander [8] and of Leo and Sekerka [9] on the composition of a misfitting precipitate.



(a) Without Elasticity



(b) With Elasticity

Fig. 1. Schemata of the composition profile in the matrix and precipitate phases during growth in (a) non-misfitting and (b) misfitting systems. The solid curve in the matrix shows the profile considered in the theories of (a) ZF and (b) LJ. Due to capillarity, the profile would be given by the dashed curve.

(b) Many phase field models (including the one used in this study) make use of a phase field variable η whose primary role is to help distinguish one phase from the other. In some settings such as precipitation of an ordered phase, η may be associated with a long-range order parameter. In other settings (such as in the present work, or in solidification), η lacks a direct physical significance, and its role in the model is justified through mathematical convenience. In such cases, it is important that the computational models reproduces well-known results from analytical theories, before they are deployed in studies of more realistic systems where the latter cannot be used.

Our study is organized as follows: Section 2 presents an outline of our phase field model. In Section 3, we first establish the essential correctness of the use of a phase field variable η through a critical comparison of its results against those of 1D ZF theory, in which capillarity and elastic effects are absent. We then use the same model to study the growth of non-misfitting and misfitting circular precipitates, and critically compare our results with those from ZF and LJ theories. These results are analyzed for elucidating the elastic and capillarity effects. These results are critically discussed in Section 4, followed by a set of conclusions in Section 5.

2 Phase Field Model

2.1 Formulation

We consider a binary alloy at constant temperature; an isolated precipitate of phase p grows into a matrix phase m . We normalize compositions in such a way that the scaled equilibrium compositions of m and p phases are zero

and unity respectively. A two-phase microstructure in this alloy is described in terms of composition $c(\mathbf{r}, t)$ (conserved variable) and order parameter $\eta(\mathbf{r}, t)$ (non-conserved variable) in a periodic domain. The order parameter field η is defined in such a way that $\eta = 0$ in the m -phase and $\eta = 1$ in the p -phase; see Eq. 6 below.

The microstructural evolution in our system is governed by the Cahn-Hilliard equation [10] and the Allen-Cahn equation [11]:

$$\frac{\partial c}{\partial t} = \nabla \cdot M \nabla \mu, \quad (1)$$

$$\frac{\partial \eta}{\partial t} = -L \frac{\delta(F/N_V)}{\delta \eta}, \quad (2)$$

where, M is the atomic mobility, μ is the chemical potential and L is the interface mobility. Chemical potential μ is defined as the variational derivative of the total free energy per atom, F , with respect to the local composition c ,

$$\mu = \frac{\delta(F/N_V)}{\delta c}. \quad (3)$$

The total free energy of the system F is assumed to be given by the sum of a chemical contribution F^{ch} and an elastic contribution F^{el} :

$$F = F^{ch} + F^{el}. \quad (4)$$

The chemical contribution F^{ch} is given by the following functional:

$$F^{ch} = N_V \int_{\Omega} [f(c, \eta) + \kappa_c (\nabla c)^2 + \kappa_\eta (\nabla \eta)^2] d\Omega, \quad (5)$$

where $f(c, \eta)$ is the bulk free energy density of the system, κ_c and κ_η are the gradient energy coefficients for gradients in composition and order parameter, respectively, and N_V is the number of atoms per unit volume.

The bulk free energy density $f(c, \eta)$ is given by,

$$f(c, \eta) = f^m(c) \left(1 - W(\eta)\right) + f^p(c)W(\eta) + P\eta^2 \left(1 - \eta\right)^2, \quad (6)$$

where P , a constant, sets the height of the free energy barrier between the m -phase and p -phase.

In Eq. 6, $f^m(c)$ and $f^p(c)$ stand for free energies of m (matrix phase) and p (precipitate) phases respectively. In our work, they are assumed to take the following simple forms:

$$f^m(c) = Ac^2, \quad (7)$$

$$f^p(c) = B(1 - c)^2 \quad (8)$$

with positive constants A and B . In Eq. 6, $W(\eta)$ is an interpolation function [12], given by:

$$W(\eta) = \begin{cases} 0; & \text{for } \eta < 0, \\ \eta^3(10 - 15\eta + 6\eta^2); & \text{for } 0 \leq \eta \leq 1, \\ 1; & \text{for } \eta > 1. \end{cases} \quad (9)$$

The elastic contribution to the free energy is:

$$F^{el} = \frac{1}{2} \int_{\Omega} \sigma_{ij}^{el} \epsilon_{ij}^{el} d\Omega \quad (10)$$

where

$$\epsilon_{ij}^{el} = \epsilon_{ij} - \epsilon_{ij}^0, \quad (11)$$

σ^{el} and ϵ^{el} are elastic stress and strain tensors respectively, and ϵ^0 is the the position dependent eigenstrain (misfit strain). The total strain ϵ_{ij} is:

$$\epsilon_{ij} = \frac{1}{2} \left\{ \frac{\partial u_i}{\partial r_j} + \frac{\partial u_j}{\partial r_i} \right\}, \quad (12)$$

where, u_i is the the displacement field.

Assuming both the m and p phases to be linear elastic, we have:

$$\sigma_{kl}^{el} = C_{ijkl} \varepsilon_{ij}^{el}, \quad (13)$$

where C_{ijkl} is the elastic modulus tensor.

The stress field σ_{ij}^{el} obeys the equation of mechanical equilibrium:

$$\sigma_{ij,j}^{el} = 0. \quad (14)$$

The eigenstrain ε_{ij}^0 and the elastic moduli C_{ijkl} are assumed to depend on order parameter as follows:

$$\varepsilon_{ij}^0(\eta) = \beta(\eta) \varepsilon^T \delta_{ij}, \quad (15)$$

$$C_{ijkl}(\eta) = C_{ijkl}^{\text{eff}} + \gamma(\eta) \Delta C_{ijkl}, \quad (16)$$

where ε^T is a constant that determines the strength of the eigenstrain, δ_{ij} is the Kronecker delta, $\beta(\eta)$ and $\gamma(\eta)$ are scalar (interpolation) functions, where, C_{ijkl}^{eff} is an “effective” modulus, C_{ijkl}^p and C_{ijkl}^m are the elastic moduli tensor of the p and m phases respectively and $\Delta C_{ijkl} = C_{ijkl}^p - C_{ijkl}^m$. All the model parameters used in our simulations are listed in their non-dimensional form in Table 1. Our non-dimensionalization procedure is the same as that used in Ref. [13].

For a configuration at time t , the equation of mechanical equilibrium, Eq. 14, is solved using an iterative Fourier spectral technique with periodic boundary conditions (described in detail in Gururajan and Abinandanan [13]; see also Refs. [14–18]) to yield the elastic stress and strain fields; these, in turn, are used to integrate the Cahn-Hilliard (Eq. 1) and Cahn-Allen (Eq. 2) equations over a

time step Δt to yield the configuration at $t + \Delta t$. For this time integration step, we use a semi-implicit Fourier spectral technique, due to Chen et al [19]; the Fourier transforms are performed using the fftw-package developed by Frigo and Johnson [20]. Microstructural evolution is simulated through a repeated application of this procedure on the new configuration at the end of each time-step.

3 Results

In our simulations, we place a small particle of initial radius R_o and composition c_e^p at the centre of our simulation cell with periodic boundary conditions; the initial composition outside the particle is set to c_∞ everywhere; with the normalizing scheme we have used, c_∞ is numerically the same as the supersaturation (or, equilibrium volume fraction) $\xi = (c_\infty - c_e^m)/(c_e^p - c_e^m)$. As the simulation proceeds, we track the particle radius, operationally defined as the distance from the centre where $\eta = 0.5$, and hence the growth coefficient α . The simulations end when either the diffusion field or the elastic stress field from neighbouring simulation cells begin to overlap; the value of α obtained just before the simulation ends is used in the plots.

3.1 Zener-Frank Theory

We first compare our 1D simulation results with those from the Zener-Frank theory. In (Fig. 2), we have plotted the growth coefficient α against matrix supersaturation ξ . The data points from our 1D simulations are in excellent agreement with the analytical results of ZF theory for 1D systems (the lowest

Table 1

Parameters used in the simulations

Parameter Type	Parameters	Non-dimensional values
Elastic Parameters	G^m/N_V	800
	ν	0.3
	A_z	1.0
	δ	0.5, 1.0 and 2.0
	ε^T	0.01
	α	$c^3(10 - 15c + 6c^2) - \frac{1}{2}$
	β	$c^3(10 - 15c + 6c^2)$
	C_{eff}^{ijkl}	$\frac{1}{2}(C_m^{ijkl} + C_p^{ijkl})$
Simulation Parameters	Δx	0.4
	Δy	0.4
	Δt	0.2
	System size	1024X1024
		2048X2048
	Allowed error in displacements	$\leq 10^{-8}$

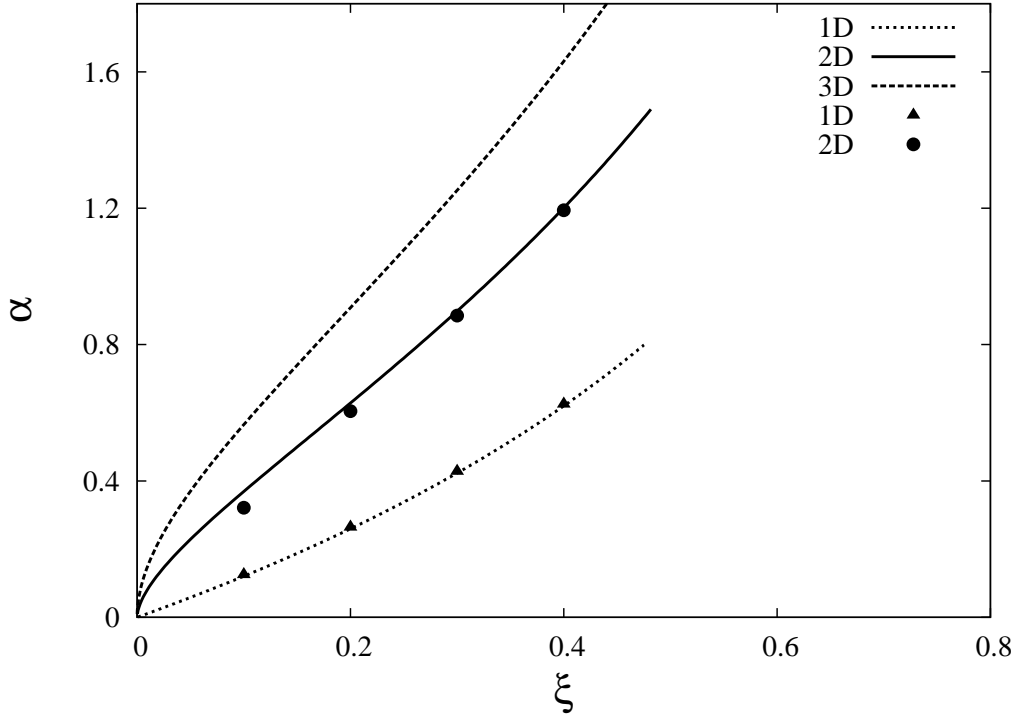


Fig. 2. Dependence of growth coefficient α on matrix supersaturation ξ . The three curves are from the ZF (sharp interface) theory for growth in 1D, 2D and 3D. The data points are from our 1D and 2D phase field simulations. In the legend, S and P stand for sharp interface theory and phase field simulations, respectively.

curve) for all supersaturations. This agreement is not just in the growth coefficient, but also in the composition profile in the matrix phase in Fig. 2 and Fig. 3(a).

Thus, this excellent agreement in the baseline case – the one without interface curvature and without misfit strains – is our main evidence for the essential correctness of the use of a phase field variable η in our model.

Fig. 2 also displays a comparison of the 2D growth coefficients from the ZF theory and our simulations. Values of α from our simulation are in excellent agreement with those from ZF theory for a supersaturation of $\xi = 0.4$ (within 0.4% at a final particle size of $R_f = 60$), but becomes less so at lower supersat-

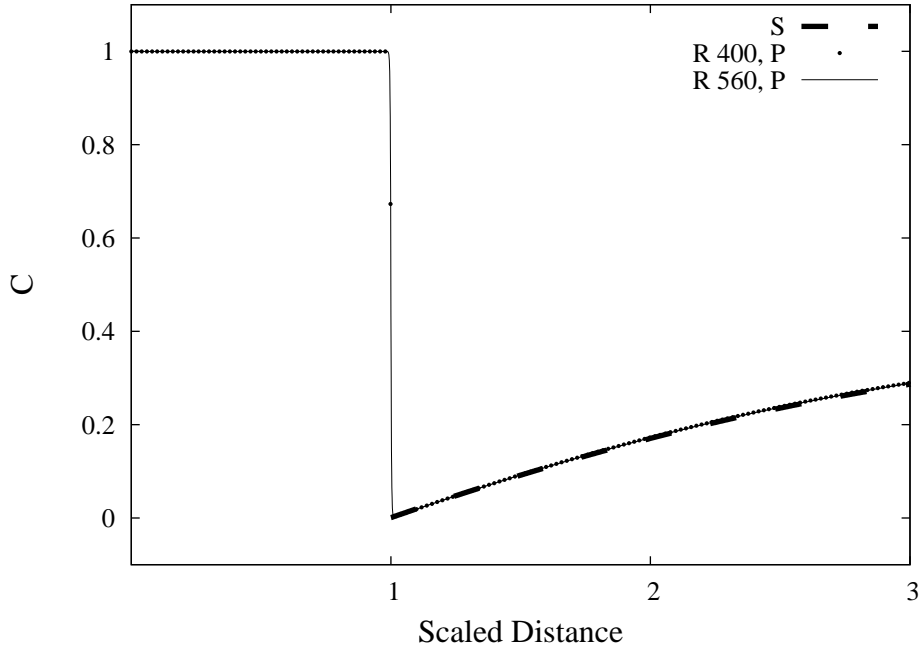
urations. At $\xi = 0.1$, growth coefficients from Z-F theory and our simulations differ by about 13 % at $R_f = 21$. The main conclusion from these results is that small particle sizes, which experience a stronger effect due to interface curvature, grow slower than predicted by ZF theory.

As shown in Fig. 1a, the curvature effect may be explained using the elevation of matrix interfacial composition from c_e^m from zero to c_I^m , which results in a reduced supersaturation. Since the reduction in supersaturation for a given particle size is a larger fraction of the original supersaturation in a less concentrated matrix, the curvature effect on growth coefficient is much higher at $\xi = 0.1$ than at $\xi = 0.4$. Thus, in Fig. 4 where the instantaneous values of growth coefficient is plotted against instantaneous particle size, the data points from our simulations are much closer to the ZF result in the latter, even at a particle size of $R = 20$. We return to a discussion of the curvature effect in Section 4.

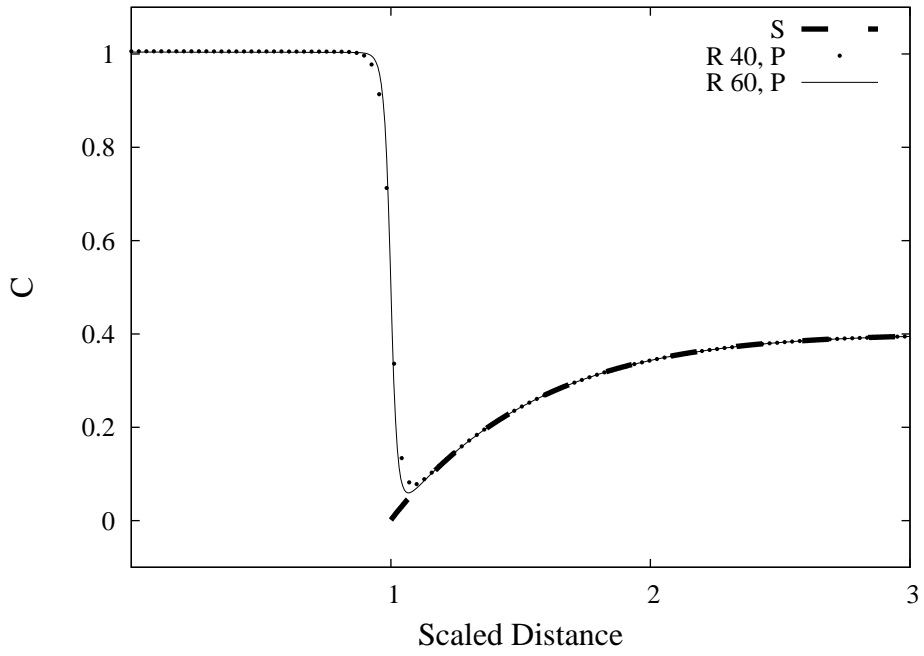
Similar to the 1D case in Fig. 3(a), the composition profile in the matrix at two different sizes obtained from our simulations show good agreement, in Fig. 3(b), with that from the Z-F theory for a matrix composition of $\xi = 0.4$.

3.2 *Effect of a misfit strain: Laroia-Johnson Theory*

In these simulations, we have used a dilatational misfit of 1 percent. The precipitate and matrix phases are elastically isotropic, with a Poisson's ratio of 0.3. The shear moduli of the two phases, however, can be different. We have considered three different cases with $(\mu_p/\mu_m) = \delta = 0.5, 1.0$ and 2.0 , though, for the sake of clarity, we present our plots only for $\delta = 0.5$.



(a) One Dimensional



(b) Two Dimensional

Fig. 3. A comparison of scaled composition profiles in (a) 1D and (b) 2D in a system with $\xi = 0.4$. The dashed curve in the matrix is from the ZF sharp interface theory, while the solid and dotted curves are from phase field simulations at two different particle sizes. The distance on the x-axis is scaled by the instantaneous particle size.

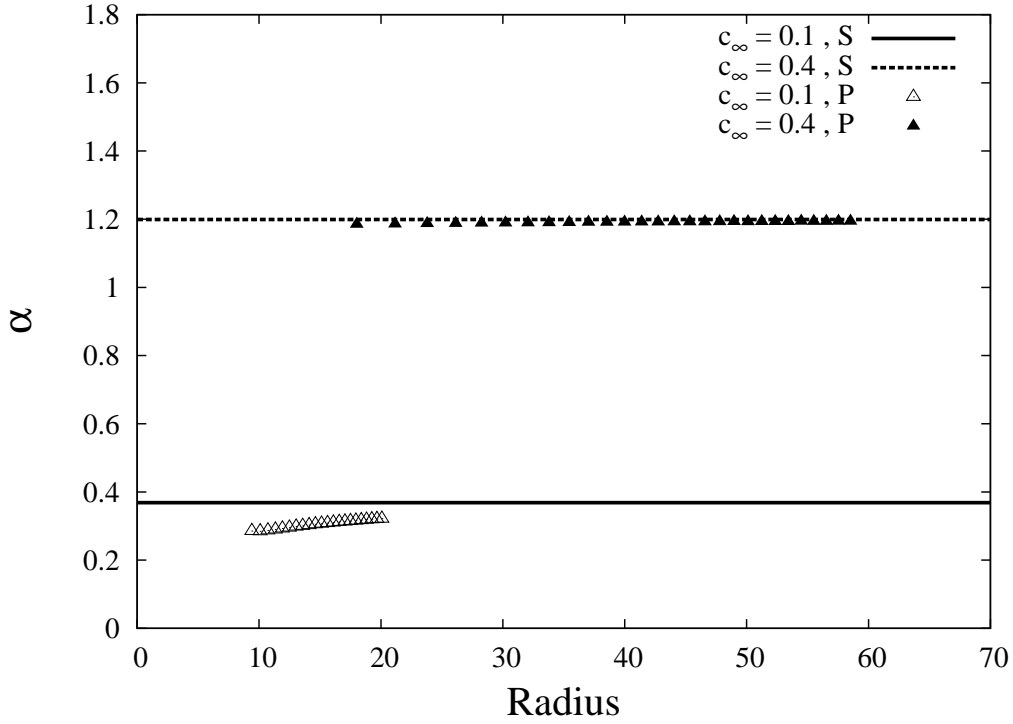


Fig. 4. Effect of capillarity on instantaneous growth coefficient α , plotted as a function of instantaneous particle radius R in 2D, non-misfitting systems. The horizontal lines are from the ZF sharp interface theory (without considering capillarity effects), and the data points are from our 2D phase field simulations.

As we mentioned in Section 1, if curvature effects are neglected, the growth coefficient vs. supersaturation curve (dashed curve in Fig. 6) from the LJ theory for the misfitting case is obtained by shifting the ZF curve (solid curve, for the non-misfitting case) to the right by c_E^m .

In Fig. 6, the growth coefficients α from our simulations are plotted against supersaturation, along with the LJ result for a system with elastically soft precipitates ($\delta = 0.5$). The agreement is quite good at high supersaturations (with a difference of just 0.1 % at a particle size of $R = 57$ in an alloy with $\xi = 0.4$). With decreasing solute concentration, however, the agreement becomes worse; at $\xi = 0.1$, for example, the difference between LJ theory and

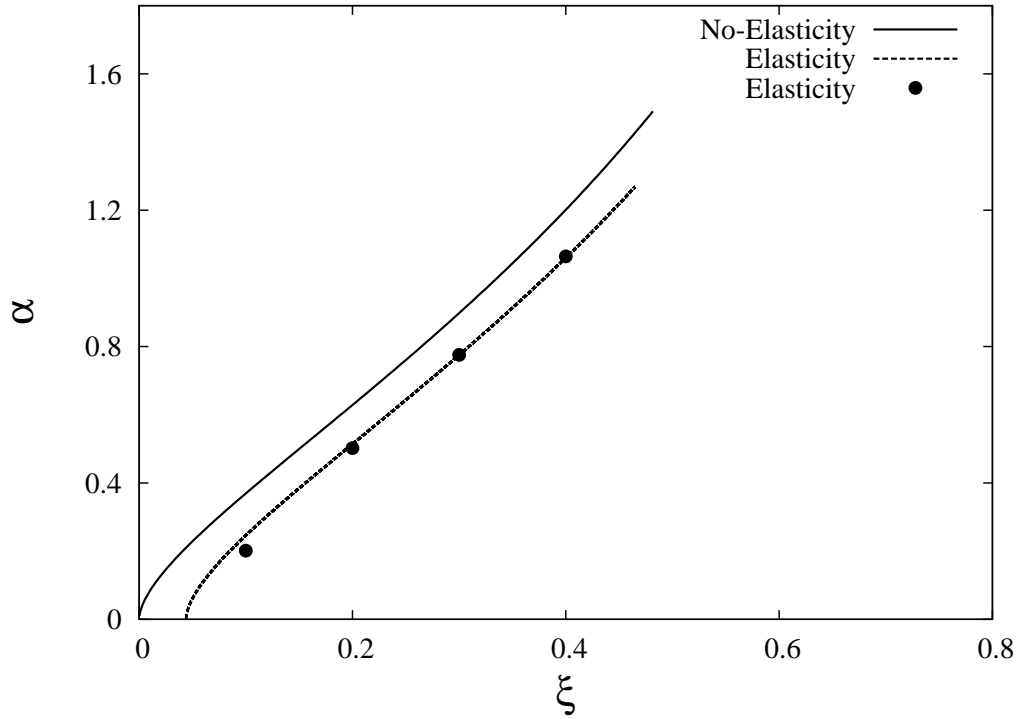


Fig. 5. Dependence of growth coefficient α on matrix supersaturation ξ in a misfitting system with $\delta = 0.5$. The dashed curve is for LJ sharp interface theory in 2D, and the data points are from 2D simulations. The solid curve, from the 2D ZF theory for non-misfitting precipitates, is also shown for comparison.

Fig. 6. Diffusion growth function for a two dimensional system modified for elastic inhomogeneity $\delta = 0.5$, along with phase field results. The lines are from the sharp interface theory, and symbols are from phase field simulations.

simulations is about 18% at $R = 21$ and $\delta = 0.5$. Thus, the combined effect of misfit and capillarity in Fig. 6 mimics that of capillarity alone in Fig.2.

In Fig. 7, we find a good agreement between the simulated (scaled) composition profile for two different times with that for the LJ model. This agreement is similar to that for the non-misfitting case in Fig. 3b.

Table 2

Precipitate growth coefficients(α) for different supersaturations(c_∞) and elastic misfit(δ)

Misfit Type	c_∞	Radius	α Analytical	α Simulation	Error (%)
Without Misfit	0.1	21	0.369	0.321	-13.01
	0.2	35	0.628	0.604	-03.82
	0.3	48	0.897	0.885	-01.34
	0.4	60	1.199	1.194	-00.42
Soft Precipitate $\delta = 0.5$	0.1	21	0.246	0.202	-17.89
	0.2	32	0.514	0.502	-02.33
	0.3	44	0.775	0.776	+00.13
	0.4	57	1.061	1.060	-00.09
Inclusion $\delta = 1.0$	0.1	19	0.208	0.145	-30.29
	0.2	31	0.482	0.469	-02.70
	0.3	43	0.742	0.744	+00.27
	0.4	56	1.023	1.031	+00.78
Hard Precipitate $\delta = 2.0$	0.1	16	0.178	0.068	-61.80
	0.2	30	0.458	0.444	-03.06
	0.3	42	0.717	0.722	+00.70
	0.4	55	0.996	1.003	+00.70

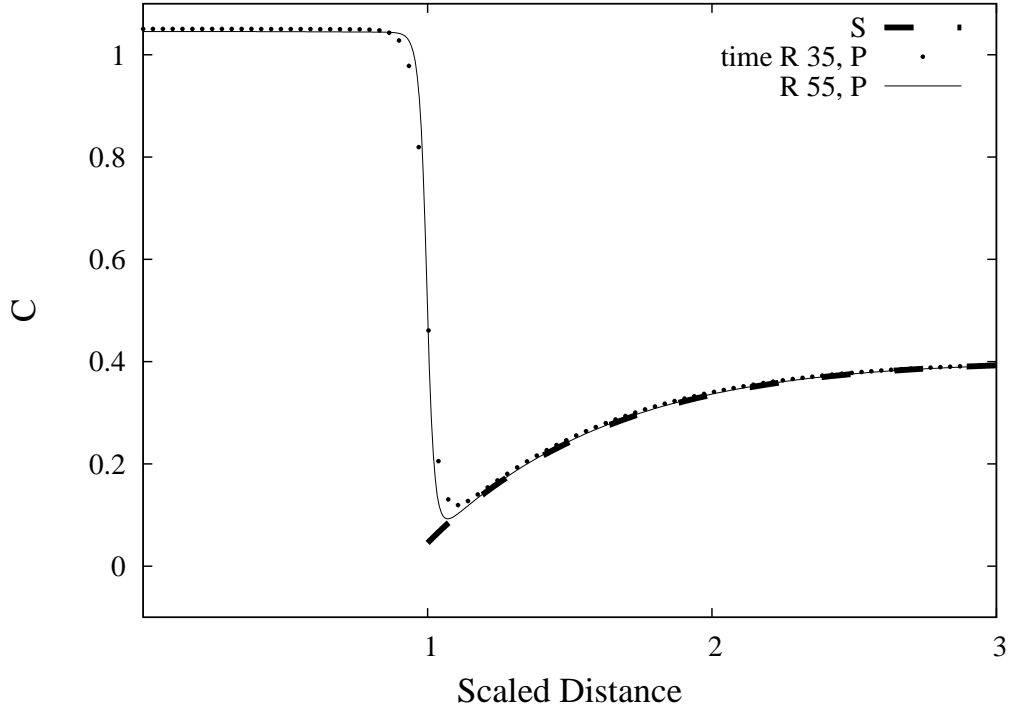


Fig. 7. A comparison of scaled composition profiles in a 2D misfitting system with $\xi = 0.4$. The dashed curve in the matrix is from the ZF sharp interface theory, while the solid and dotted curves are from phase field simulations at two different particle sizes. The distance on the x-axis is scaled by the instantaneous particle size.

3.3 Effect of interface curvature

A more detailed assessment of the role of capillarity is possible by considering c_I^p , the precipitate interfacial composition. In the sharp interface model, the difference $\Delta c_I^p = (c_I^p - c_e^p)$, is proportional to $\Delta c_I^\alpha = (c_I^\alpha - c_e^\alpha)$:

$$\Delta c_I^p = \frac{\Psi^m}{\Psi^p} \Delta c_I^\alpha \quad (17)$$

where $\Psi = [\partial^2 f / \partial c^2]_{c_e}$ in the designated phase, and Δc_I^m is given by the generalized Gibbs-Thomson effect [21]:

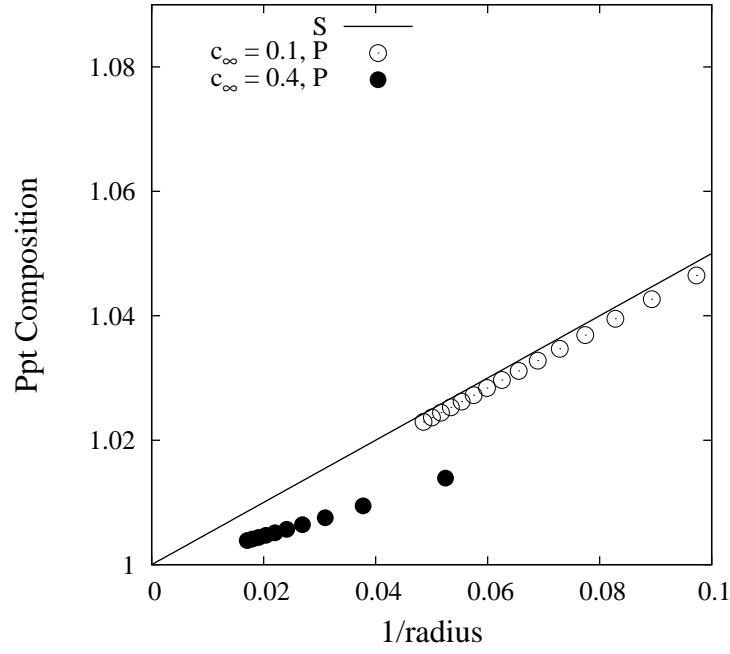
$$\Delta c_I^m = \frac{\sigma_{ij}^m (\varepsilon_{ij}^m - \varepsilon_{ij}^p) + [\sigma_{ij}^p (\varepsilon_{ij}^p - \varepsilon^T \delta_{ij}) - \sigma_{ij}^m \varepsilon_{ij}^m] / 2}{(c_e^p - c_e^m) \Psi^m} + \frac{\chi \gamma}{(c_e^p - c_e^m) \Psi^m}. \quad (18)$$

In the above equation, σ_{ij} and ε_{ij} are the stresses and strains, respectively, in the designated phase, ε^T is the dilatational eigenstrain and χ is the mean interface curvature. In our 2D simulations, $\chi = 1/R$; from Eq. 7 and Eq. 8 (with the parameter values of $A = B = 1$), we get $\Psi^m = \Psi^p = 2$. For the values of misfit, shear modulus and Poisson's ratio used in this study (see Table 1), the (constant) elasticity contribution to ΔC_I^m – the first term on the right hand side of Eq. 18) – is 0.044, 0.056 or 0.066 for systems with $\delta = (\mu_p / \mu_m) = 0.5, 1.0$ or 2.0, respectively.

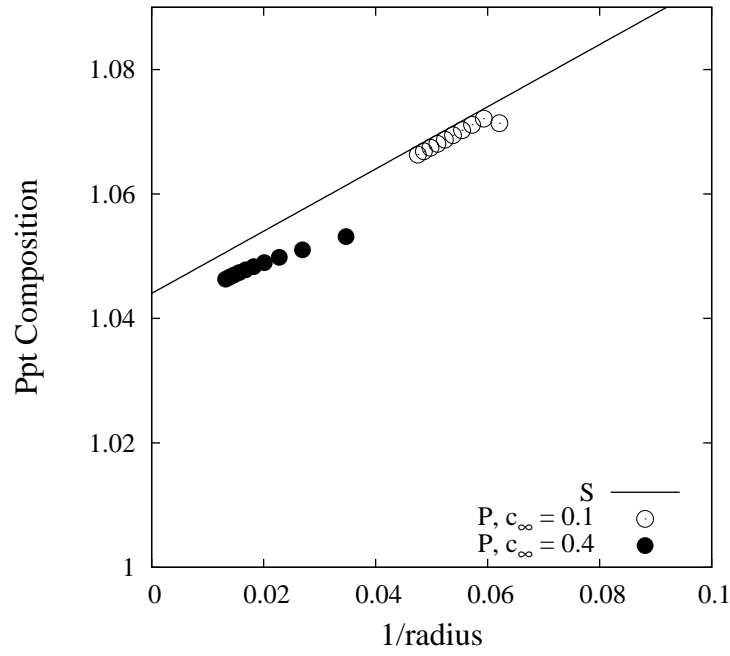
In simulations using diffuse interface models, interfacial compositions c_I^p and c_I^m cannot be measured, as the composition changes continuously across an interface region of finite width. However, if we assume that the chemical potential gradients are negligible inside the precipitate, the composition anywhere in the precipitate should be the same as c_I^p .

In Fig. 8, we have plotted c_I^p , obtained from simulations against the inverse of particle size R in (a) non-misfitting and (b) misfitting systems. In Fig. 8a, the straight line represents the Gibbs-Thompson result (Eq. 18 without the stress and strain terms), and the data points are from our simulations; for clarity, we have presented data only for two supersaturations: $\xi = 0.1$ and $\xi = 0.4$. This figure shows that, in a growth setting, particles growing in more concentrated alloys display a smaller Gibbs-Thompson effect.

In Fig. 8b, we compare the theoretical value of c_I^p (the dashed line) with those



(a) One Dimensional



(b) Two Dimensional

Fig. 8. Dependence of precipitate composition on particle radius in (a) non-misfitting and (b) misfitting systems. The straight line is for c_I^p , precipitate composition at a curved interface, given by the Gibbs-Thomson effect (see Eqs. 17 and 18). The data points are from our simulations with $\xi = 0.1$ (open circles) and $\xi = 0.4$ (filled circles).

from simulations for $\xi = 0.1$ and $\xi = 0.4$. This figure also shows that the Gibbs-Thompson effect is less completely realized for more supersaturated alloys, leading to a better match between α from simulations and that from theory (see Fig. 2 and 6).

Thus, Fig. 8 reveals yet another reason for the closer agreement between ZF theory and our 2D simulations for more concentrated alloys: Gibbs-Thompson effect is less completely realized in systems with a higher supersaturation.

At $\xi = 0.1$, even though our results were obtained in a growth setting, the small supersaturation ensures that the precipitate experiences a large part of the Gibbs-Thomson effect is realized. Thus, we find a good agreement in c_7^p values from simulations with those calculated from Eq. 18. This agreement in Fig. 8b may be taken as an indirect verification of the predictions of Johnson and Alexander [8] and Leo and Sekerka [9] on the phase compositions across a sharp interface.

4 Discussion

As we mentioned in Section 1, the primary aim of this paper is to use our ‘computer experiments’ to validate the Laraia-Johnson (LJ) theory of elastic stress effects during precipitate growth. The following features of our phase field model make it resemble closely the alloy model used in the LJ theory: isotropic interfacial energy, isotropic atomic mobility, constant atomic diffusivity in the matrix (and in the precipitate too, though it’s not an essential part of the LJ theory), and constant misfit the precipitate phase. While LJ theory includes cases where composition gradients may engender stress, our

model parameters are such that they do not.

However, interfacial curvature (and hence, the Gibbs-Thomson effect) is one feature which is always present in phase field simulations (except in 1D), but absent in LJ and ZF theories. Its primary consequence is to dampen the growth rate. However, this dampening effect keeps decreasing with increasing particle size, and the instantaneous growth coefficient keeps rising towards that predicted by ZF and LJ theories (see Fig. 4).

Our 2D simulations (with and without misfit) show that the Gibbs-Thompson effect is only partially realized during growth, especially at large supersaturations. Since Gibbs-Thompson effect dampens the growth rate, its partial realization helps bring the growth rate closer to the theoretically predicted rate in these alloys – see Figs. 2 and 6 for 2D growth.

Clearly, with higher (lower) atomic mobility in the p phase, Gibbs-Thompson effect can be realized more (less) completely. Thus, if the atomic mobility in the p phase is higher (lower), the approach of the growth coefficient (in Fig. 4) towards the ZF or LJ result will be delayed (hastened) to larger precipitate sizes. Our simulations, however, cannot address this issue, since they use a constant mobility in both m and p phases.

Finally, we turn to other similar studies that compared results from sharp and diffuse interface models. Specifically, we mention Chen and co-workers, who have compared their phase field results on diffusion fields around a precipitate with those obtained by solving a diffusion equation. However, the focus of their work was on diffusion fields in ternary systems [22] or on lengthening and thickening of plate-like precipitates [23].

5 Conclusion

- (1) Using our phase field simulations as 'computer experiments', we have validated the Laraia-Johnson theory of growth of misfitting particles in systems in which composition differences do not engender stress.
- (2) Capillarity effects decrease instantaneous growth rates, with this dampening effect being more pronounced at smaller sizes and at smaller supersaturations.
- (3) At constant particle size, capillarity has a smaller effect in alloys with larger supersaturations, because Gibbs-Thomson effect is less completely realized.
- (4) At low supersaturations, the Gibbs-Thomson effect is more completely realized, and our results on precipitate compositions are in agreement with those predicted from the theory of thermodynamics of stressed solids.

Acknowledgements

The authors thank the Volkswagen Foundation for financial support for this work. They also thank Prof. V. Jayaram and Dr. H. Ramanarayan for discussions.

References

- [1] C. Zener, Theory of growth of spherical precipitates from solid solution, *Journal of Applied Physics* 20 (10) (1949) 950–953.
- [2] F. C. Frank, Radially symmetric phase growth controlled by diffusion,

- Proceedings of the Royal Society of London. Series A, Mathematical and Physical Sciences 201 (1067) (1950) 586–599.
- [3] J. D. Eshelby, The determination of the elastic field of an ellipsoidal inclusion, and related problems, Proceedings of the Royal Society of London. Series A, Mathematical and Physical Sciences (1934-1990) 241 (1226) (1957) 376–396.
- [4] F. Larche, J. W. Cahn, A linear theory of thermochemical equilibrium of solids under stress, *Acta Metallurgica* 21 (8) (1973) 1051–1063.
- [5] F. Larche, J. Cahn, The effect of self-stress on diffusion in solids, *Acta Metallurgica* 30 (10) (1982) 1835–1846.
- [6] J. W. Cahn, F. C. Larche, A simple model for coherent equilibrium, *Acta Metallurgica* 32 (11) (1984) 1915–1923.
- [7] F. C. Larche, J. W. Cahn, The interactions of composition and stress in crystalline solids, *Acta Metallurgica* 33 (3) (1985) 331–357.
- [8] W. C. Johnson, J. I. D. Alexander, Interfacial conditions for thermomechanical equilibrium in two-phase crystals, *Journal of Applied Physics* 59 (8) (1986) 2735–2746.
- [9] P. Leo, R. F. Sekerka, The effect of surface stress on crystal-melt and crystal-crystal equilibrium, *Acta Metallurgica* 37 (12) (1989) 3119 – 3138.
- [10] J. W. Cahn, On spinodal decomposition, *Acta Metallurgica* 9 (1961) 795–801.
- [11] S. M. Allen, A microscopic theory for antiphase boundary motion and its application to antiphase domain coarsening, *Acta Metallurgica* 27 (1979) 1085–1095.
- [12] S. L. Wang, R. F. Sekerka, A. A. Wheeler, B. T. Murray, S. R. Coriell, R. J. Barun, G. B. McFadden, Thermodynamically-consistent phase-field models for solidification, *Physica D* 69 (1993) 189–200.

- [13] M. P. Gururajan, T. A. Abinandanan, Phase field study of precipitate rafting under a uniaxial stress, *Acta Materialia* 55 (2007) 5015–5026.
- [14] A. Anthoine, Derivation of the in-plane elastic characteristics of masonry through homogenization theory, *International journal of solids and structures* 32 (2) (1995) 137–163.
- [15] H. Moulinec, P. Suquet, A numerical method for computing the overall response of nonlinear composites with complex microstructure, *Computer methods in applied mechanics and engineering* 157 (1) (1998) 69–94.
- [16] H. Michel, J. C. and Moulinec, P. Suquet, Effective properties of composite materials with periodic microstructure: a computational approach, *Computer Methods in Applied Mechanics and Engineering* 172 (1) (1999) 109–143.
- [17] S. Y. Hu, L. Q. Chen, A phase-field model for evolving microstructures with strong elastic inhomogeneity, *Acta Materialia* 49 (11) (2001) 1879–1890.
- [18] J. Zhu, L.-Q. Chen, J. Shen, Morphological evolution during phase separation and coarsening with strong inhomogeneous elasticity, *Modelling and Simulation in Materials Science and Engineering* 9 (6) (2001) 499–511.
- [19] L. Q. Chen, J. Shen, Applications of semi-implicit fourier-spectral method to phase field equations, *Computer Physics Communications* 108 (2) (1998) 147–158.
- [20] M. Frigo, S. G. Johnson, FFTW: an adaptive software architecture for the FFT (<http://www.fftw.org>), in: *Proceedings of the 1998 IEEE International Conference on Acoustics, Speech and Signal Processing*, Vol. 3, 1998, pp. 1381–1384.
- [21] W. Johnson, Precipitate shape evolution under applied stress - thermodynamics and kinetics, *Metallurgical Transactions A* 18 (2) (1987) 233–248.

- [22] L. Q. Chen, N. Ma, K. Wu, Y. Wang, Quantitative phase field modeling of diffusion-controlled precipitate growth and dissolution in ti-al-v, *Scripta Materialia* 50 (6) (2004) 471–476.
- [23] S. Y. Hu, J. Murray, H. Weiland, Z. K. Liu, L. Q. Chen, Thermodynamic description and growth kinetics of stoichiometric precipitates in the phase-field approach, *Computer Coupling of Phase Diagrams and Thermochemistry* 31 (2) (2007) 303–312.